Surge Arrester Energy Stress at A VSC-HVDC Link Due to DC Fault Transients

Yanfei Liu, Dongsheng Zhang, Li Zhang, Tao Xue and Haoyan Xue

***Abstract*--This paper presents a comprehensive study on transient characteristics of surge arrester in a typical Voltage Source Converter - High Voltage Direct Current (VSC-HVDC) submarine cable link. The DC submarine cable bundle is modeled using the latest technique in an existing electromagnetic transient (EMT) - type simulation tool. The Modular Multilevel Converters (MMC) arm inductance, transformer reactance, MMC blocking time, power transmission level, DC fault location and DC cable model reduction are adjusted to investigate the impact on discharge current and energy absorption of DC surge arresters. Those parameters' influence on sheath (armor) voltage of DC cable is also made clear.**

***Keywords*: VSC-HVDC, Transients, Surge Arrester, Overvoltage, Fault.**

I. Introduction

GIVEN the essential advantages of Voltage Source Converter - High Voltage Direct Current (VSC-HVDC) transmission technology, such as its capability to connect with weak AC grids, it is emerging as one of the most viable configurations for high penetration of renewable energy and cross-border power delivery [1], [2].

In existing VSC configurations, Modular Multilevel Converters (MMC) show superior characteristics in terms of transient behavior compared to traditional two- or three-level topologies. These advantages have led to widespread adoption of MMC technique by utilities and industries in energy sector, significantly enhancing the deployment of submarine cable-based VSC-HVDC links [3].

Due to line to ground fault on DC side, its electromagnetic transient (EMT) can cause overvoltage issues on VSC-HVDC link. In general, the metal oxide varistor (MOV) surge arrester should be adopted into the system and limit the overvoltage on the DC submarine cable side. Also, the characteristics of discharge current and energy absorption are important for a reliable design of MOV surge arrester. More details on the DC underground cable link are presented in references [4]-[8].

In this paper, the study focuses on transient characteristics of surge arrester and cable sheath (armor) of VSC-HVDC submarine link due to a typical DC fault. The latest modeling technique [9], [10] on DC submarine cable bundle has been adopted in the study. This paper provides new findings regarding transient characteristics of DC surge arrester and cable sheath (armor) in addition to contents investigated and discussed in reference [10].

In Section II, a VSC-HVDC benchmark system [4], [10] used in this paper is explained and described. The non-linear voltage and current properties of DC surge arrester are scaled and represented. The grid components are developed using an existing EMT - type simulation software [11], [12].

In Section III, the impact of various parameters on discharge current and energy absorption of surge arrester is studied. Also, the influence on sheath (armor) voltage of DC submarine cable bundle is made clear. Moreover, the MMC arm inductance, transformer reactance, MMC blocking time, power transmission level, DC fault location and DC cable model reduction are adjusted to investigate the transients on DC surge arrester and cable sheath (armor).

The findings of this paper further provide insights that could be considered in surge arrester design and overvoltage protection of submarine cable bundle in VSC-HVDC links.

II. System Description

In this section, the VSC-HVDC submarine system used in the study is introduced. As shown in Fig. 1, the simulation circuit is built using an EMT-type simulation software (EMTP®) [12]. The source grids at the connections of VSC-HVDC are 400 kV with power frequency 50 Hz and a short circuit capacity of 10 GVA. The VSC system is based on a symmetrical and monopolar MMC topology with 400 submodules per arm [4], [5]. The rated voltage and capacity of HVDC are ±320 kV and 1000 MW. More details are given in Appendix. The active / reactive power and DC voltage / reactive power control methods are used for VSC 1 and VSC 2, respectively. The VSCs are modeled based on the switching function of arm method. As shown in Fig. 2, the DC submarine cable bundle is represented by the wideband (WB) [13], [14] or constant parameter (CP) model depending on the study. Also, the latest modeling method [9], [10] of submarine cable bundle is adopted in this paper, since no similar study exists in the current publications.

As shown in Fig. 1, the surge arresters ZnOP1, ZnOP2, ZnON1 and ZnON2 are placed at both ends of the submarine cable link. VSC 1 and VSC 2 represent rectifier and inverter sides respectively. The voltage and current nonlinear curves of installed surge arresters are illustrated in Fig. 3.

Y. Liu is with Polytechnique Montreal, Montreal, QC, Canada (e-mail: yanfei.liu@polymtl.ca).
D. Zhang and L. Zhang are with Yinchuan University of Energy, Yinchuan, China (emails: remindn@163.com and 2586501881@qq.com).
T. Xue is with the Hong Kong Polytechnic University, Hong Kong, China (email: xt-tao.xue@connect.polyu.hk).
Corresponding author: H. Xue is with Powertech Labs Inc, Surrey, BC, Canada (e-mail: haoyanxue@hotmail.com).

Paper submitted to the International Conference on Power Systems Transients (IPST2025) in Guadalajara, Mexico, June 8-12, 2025.

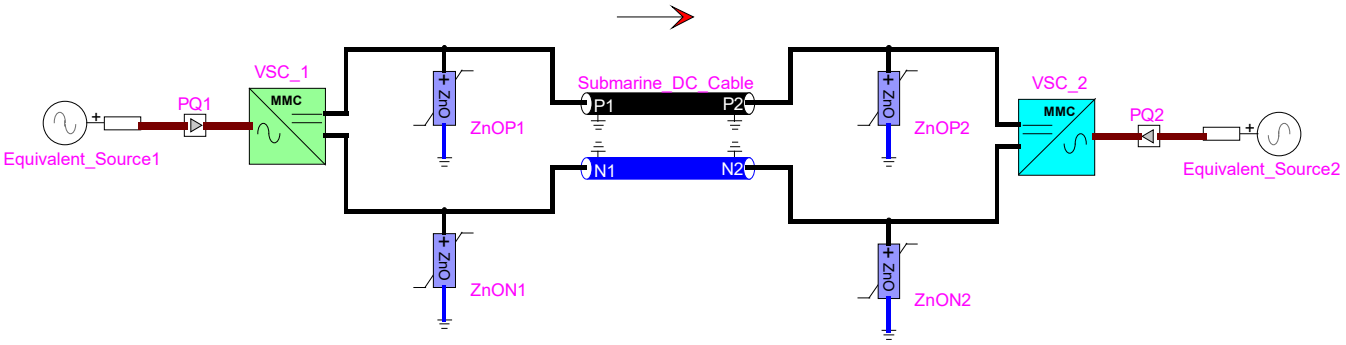

Fig. 1 A VSC-HVDC submarine cable link.

The following values are selected and scaled based on references [6], [15] for a DC surge arrester with a same voltage level. The DC pole to ground 320 kV is used as the base voltage. Since it is a HVDC system, the DC voltage can be regarded as a peak value in design of surge arrester [16].

In the following study, the maximum value of pole to ground voltage is set to 343 kV (1.07 pu), which corresponds to the leakage current at 100 μA. The maximum continuous operating voltage (MCOV) is set to 379 kV (1.18 pu). The rated voltage (U_r) is considered to be 426 kV (1.33 pu).

In general, the energy capability of AC surge arrester is specified in kJ/kV based on its root mean square (rms) rated voltage (U_r), and it typically ranges from 4 kJ/kV to 16 kJ/kV [17]. By adopting an equivalent rms concept in reference [16], which means that 426 kV is divided by 1.414 = 301 kV, the energy capability of surge arrester studied in this paper is likely located between a minimum value 1.21 MJ and a maximum value 4.82 MJ. The surge level of 578 kV (1.81 pu) is selected at 1 kA for slow-front transient area. Thus, the transient overvoltages produced by the pole to ground fault are limited to be less than the switching impulse withstand level (698 kV, 2.18 pu) designed and tested for submarine DC cables [18].

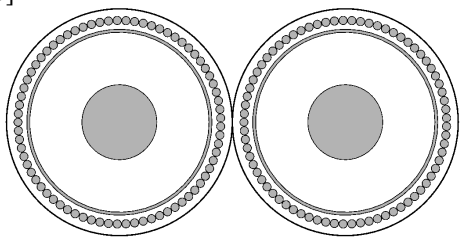

Fig. 2 A DC submarine cable bundle.

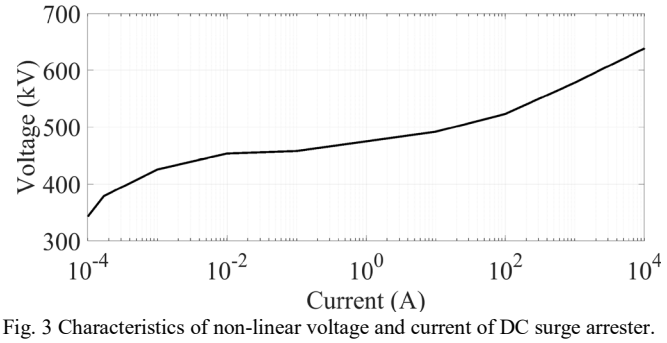

Fig. 3 Characteristics of non-linear voltage and current of DC surge arrester.

In general, the surge arrester model should be determined by transient frequency. For slow-front overvoltage and lower frequency analysis, a resistive surge arrester model can be used, in which corresponds to a non-linear resistance with representation of voltage and current characteristics. For fast-front overvoltage, the surge arrester shows an inductive effect [16]. Then, the instantaneous current peak may not correspond to the instantaneous voltage peak across the surge arrester [16]. Thus, a high frequency surge arrester model is required [16]-[20]. The slow-front overvoltage on the DC side is majorly generated by DC fault or the fault in the converter station [21]. In the following study, the resistive surge arrester model is adopted in the EMT-type simulation tool considering relatively low frequency transients, i.e., less than 1 kHz.

III. System Study Results

In this section, the transient and energy characteristics of surge arrester are studied and analyzed based on an EMT-type simulation tool. At 500 ms, a DC side permanent fault is applied at 50 km of positive pole of submarine cable, and the length of cable is 100 km. The sheath and armor of DC cable are solidly bonded and grounded through grounding resistance 1 Ω at sending and receiving ends.

The protection of HVDC system consists of DC overcurrent and detection of deep voltage sag. The margin of DC overcurrent is set to 2.3 pu. The VSC station is blocked, and the main AC circuit breaker is tripped if the DC current protection is activated. Also, the VSC is blocked if the grid side voltage drops below 0.1 pu. The default case is investigated in Section III - A. The impact of MMC parameters, active power limit, fault location and DC cable models are further studied in Section III - B to Section III - G.

A. Impact of DC surge arrester

As shown in Fig. 4, the positive and negative pole to ground voltages are calculated at both ends of VSC converter stations. The transient voltages calculated without surge arresters are illustrated in Fig. 4 (a). The peak overvoltage appears at the negative pole of VSC 1, and it reaches -842.8 kV (-2.63 pu). Also, the faulted pole experiences higher frequency oscillations due to that the discontinuity between DC cable terminals and MMC arm inductances generate more reflections and refractions on transient waveforms. As illustrated in Fig. 4 (b), it is clear that the peak overvoltage on negative pole of VSC 2 is effectively limited to -560.1 kV (-1.75 pu).

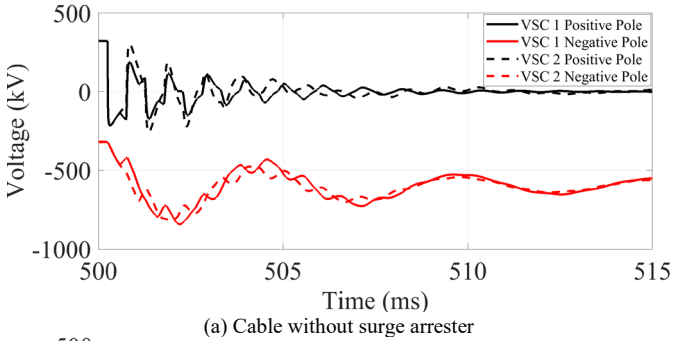

(a) Cable without surge arrester

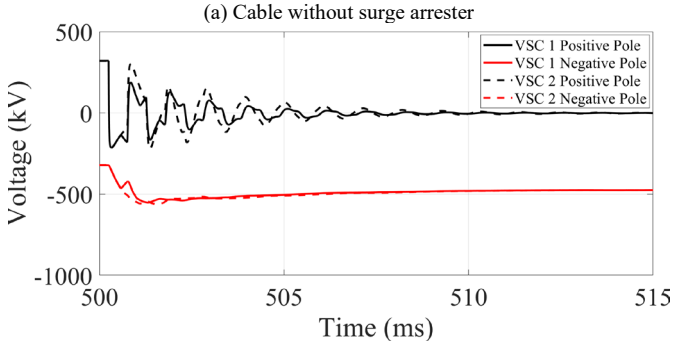

(b) Cable with surge arrester

Fig. 4 Pole to ground voltages at VSC 1 and VSC 2.

The DC currents of VSC 1 and VSC 2 are illustrated in Fig. 5. The peak value of DC current in VSC 1 and VSC 2 reaches 3.36 pu and 2.53 pu, respectively, then the VSCs are blocked due to the operation of DC overcurrent protection. Also, it is observed that the DC transient current on VSC 1 (rectifier side) has no polarity reversal, and it reaches the margin of DC current maximum limit protection faster than the DC current on VSC 2 (inverter side).

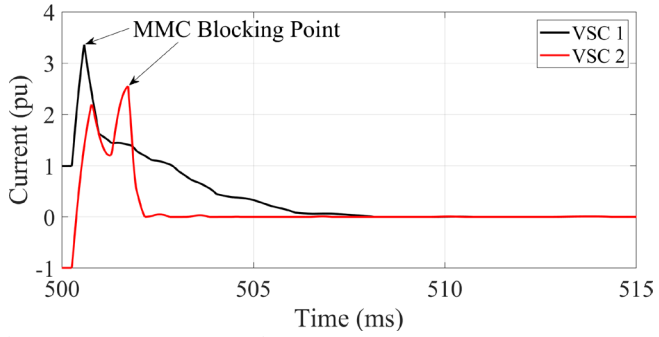

Fig. 5 DC current at VSC 1 and VSC 2.

Furthermore, the discharge current and energy absorption on surge arresters of negative pole are shown in Fig. 6. Because of VSC 1 blocking impact, the envelope of transient voltage on VSC 2 negative pole is larger than the one on VSC 1 negative pole. Thus, the inverter side surge arrester ZnON2 experiences more severe discharge and energy conditions. The positions of surge arrester are shown in Fig. 1.

The influence of surge arrester on sheath (armor) to ground voltages at both ends of DC submarine cable is shown in Fig. 7. The calculated peak sheath overvoltage appears at VSC 2 side with surge arrester, and it reached 4.42 kV. The reason is from the second peak of discharge current on ZnON2, as illustrated in Fig. 6 (a). Therefore, the discharge characteristics of surge arrester may increase overvoltage stress on DC cable sheath (armor).

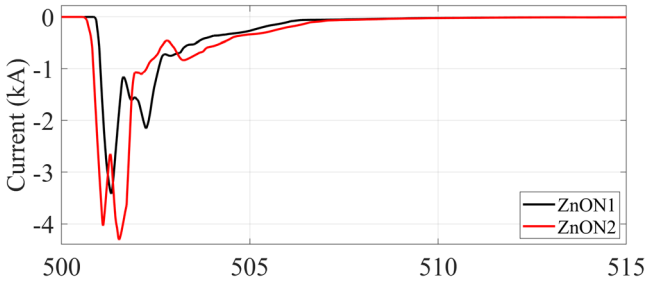

(a) Discharge current

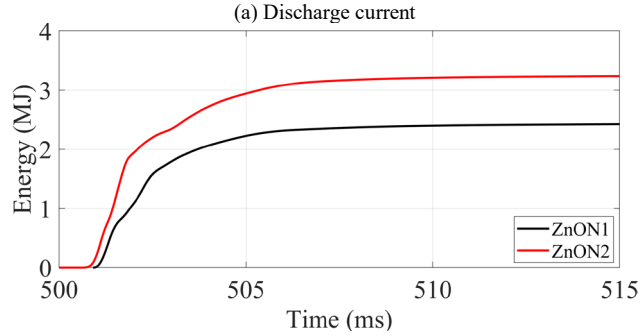

(b) Energy absorption

Fig. 6 Transient characteristics of surge arresters.

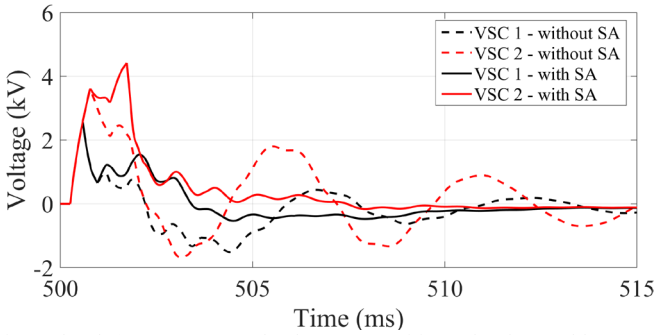

Fig. 7 Sheath (armor) to ground voltages on positive pole of DC cable at VSC 1 and VSC 2.

It should be noted that results presented here refer to a base case, and default system parameters can be found in Section III and Appendix.

In the following sections, the MMC arm inductance, transformer reactance, MMC blocking delay, active power, DC fault location and cable models are varied to study the impact on transients of surge arrester. The base case can be compared with the results obtained using various parameters.

B. Impact of MMC arm inductance

The influence of MMC arm inductance on cable sheath (armor) to ground voltage and transients of surge arrester is illustrated in Fig. 8 and Fig. 9. The MMC arm inductance H_{MMC} is tuned to 0.1 pu and 0.2 pu respectively. It is clear that the large MMC arm inductance contributes more severe discharges in surge arresters. Thus, the surge arrester experiences more critical conditions considering energy absorption.

As shown in Fig. 9, the sheath (armor) voltage calculated

using H_{MMC} = 0.2 pu gives a longer transient voltage window (up to 503.5 ms) than the results (up to 501.5 ms) calculated by H_{MMC} = 0.1 pu. The maximum sheath (armor) to ground voltage 4.5 kV is observed for H_{MMC} = 0.1 pu.

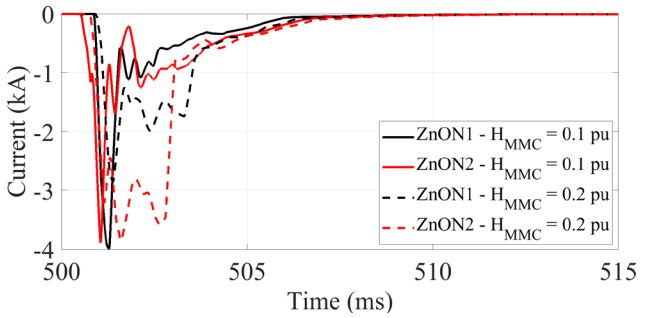

(a) Discharge current

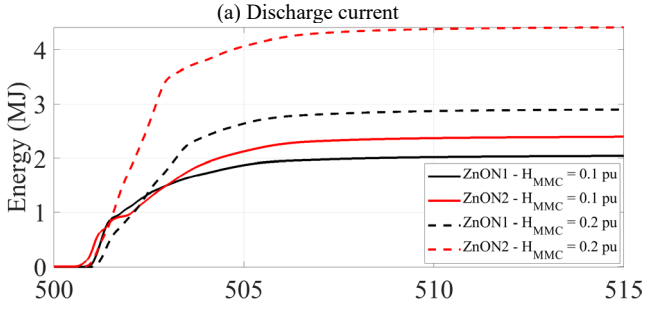

(b) Energy absorption

Fig. 8 Transient characteristics of surge arresters with different MMC arm inductances.

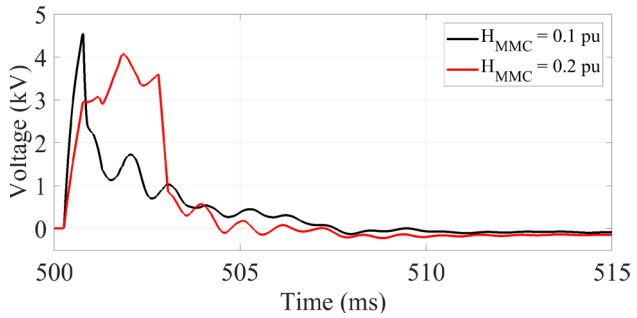

Fig. 9 Sheath (armor) to ground voltages on positive pole of DC cable at VSC 2 with different MMC arm inductances.

C. *Impact of transformer reactance*

The reactance of VSC-HVDC transformers is adjusted to 0.15 pu and 0.25 pu. The influence on discharge characteristics is shown in Fig. 10.

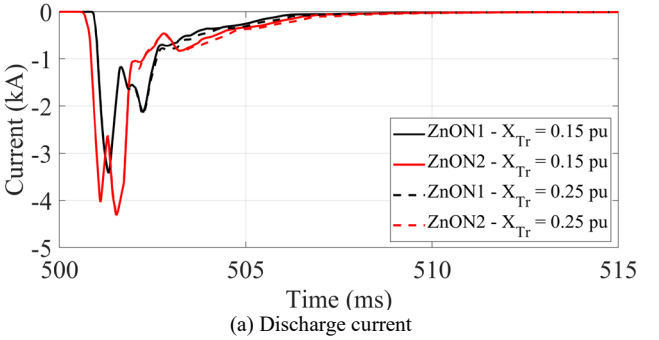

(a) Discharge current

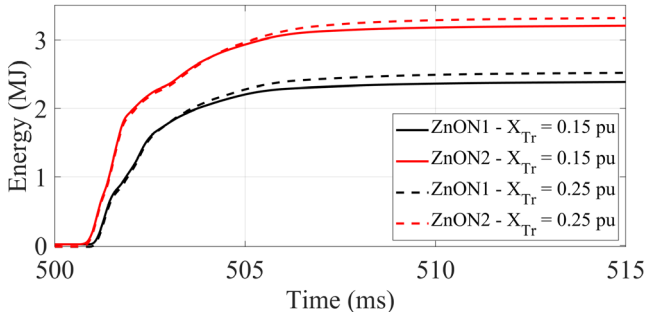

(b) Energy absorption

Fig. 10 Transient characteristics of surge arresters with different transformer reactance.

The transformer reactance shows negligible effect on the discharge current and energy absorption of surge arrester in comparison to impact of MMC arm inductance. As shown in Fig. 11, no impact is observed on sheath (armor) voltage.

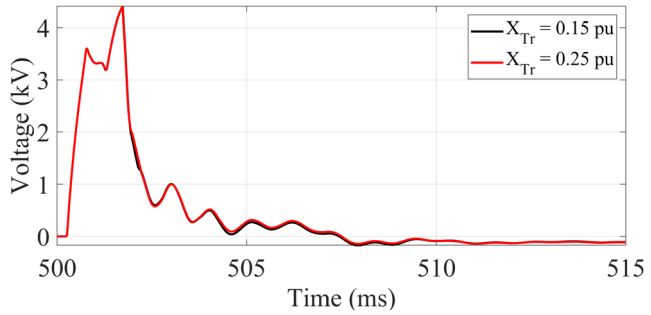

Fig. 11 Sheath (armor) to ground voltages on positive pole of DC cable at VSC 2 with different transformer reactance.

D. *Impact of MMC blocking delay*

As shown in Fig. 12, the surge arresters experience less energy discharge with small MMC blocking delay t_d. However, the peak value of discharge current is the same for the 2 different cases, i.e., -5.8 kA. It should be noted that the relatively long MMC blocking delay produces critical energy stress on surge arresters which may cause failure.

The sheath (armor) to ground voltage on positive pole of DC cable at VSC 2 is illustrated in Fig. 13. The fast MMC blocking has a shorter transient window, however, it has no impact on peak value of voltage.

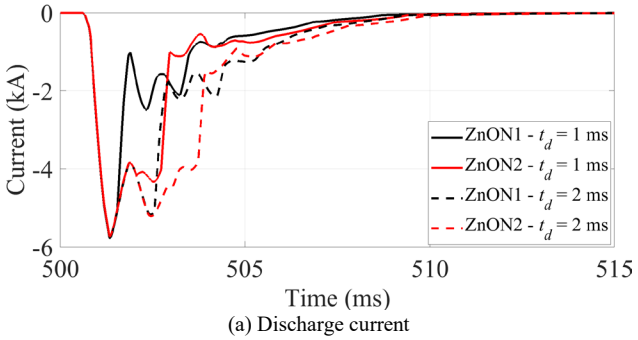

(a) Discharge current

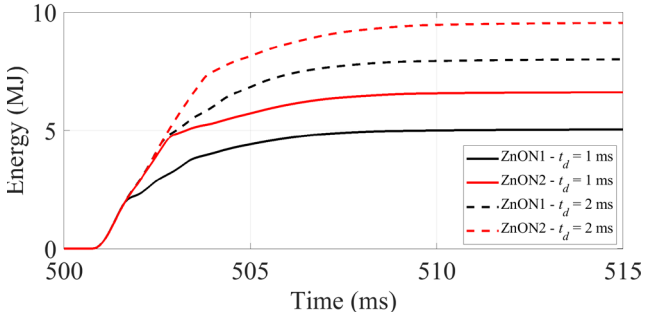

(b) Energy absorption

Fig. 12 Transient characteristics of surge arresters with different MMC blocking delays.

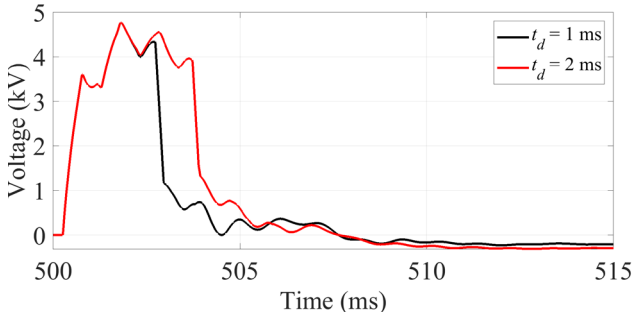

Fig. 13 Sheath (armor) to ground voltages on positive pole of DC cable at VSC 2 with different MMC blocking delays.

E. Impact of active power transfer

The active power transmitted in the DC link is set to 1 GW for the default case. The active power is further decreased to 500 MW and 100 MW respectively to check its effect.

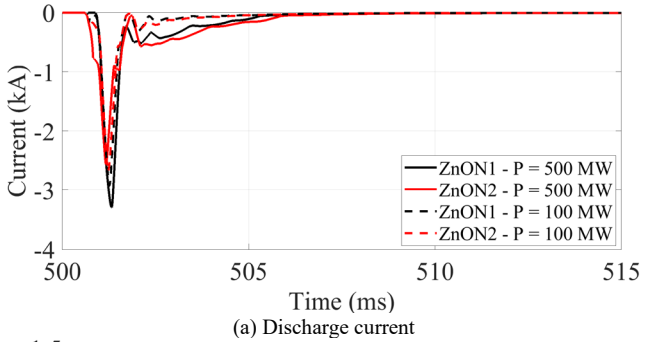

(a) Discharge current

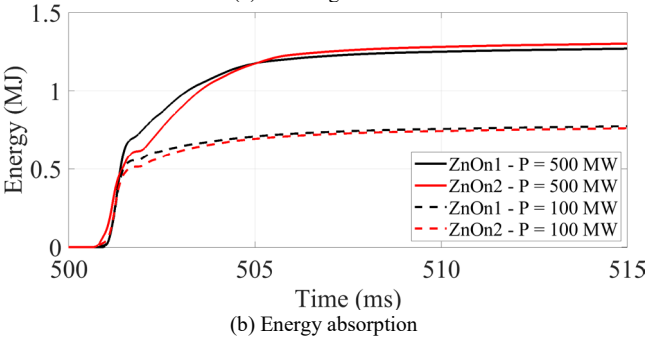

(b) Energy absorption

Fig. 14 Transient characteristics of surge arresters with different active power transfers.

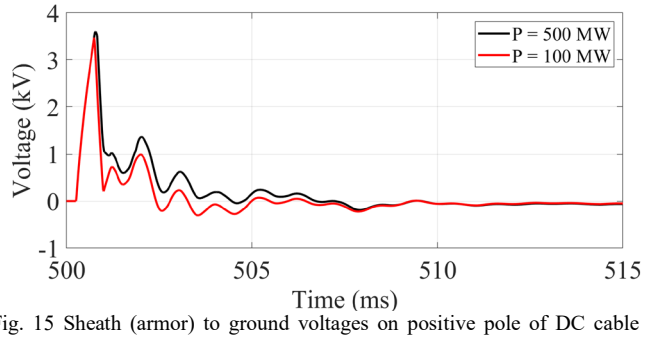

Fig. 15 Sheath (armor) to ground voltages on positive pole of DC cable at VSC 2 with different active power transfers.

As shown in Fig. 14, the discharge energy of surge arrester increases significantly as transmitted active power increases, i.e., 0.75 MJ and 1.26 MJ for 500 MW and 100 MW, respectively. As illustrated in Fig. 6, the maximum 3.55 MJ is observed for 1 GW active power delivery in the DC link. No significant impact of active power on transient voltage of sheath (armor) is observed, as shown in Fig. 15.

F. Impact of DC fault location

The location of DC fault is changed to VSC 1 (0 km), and 20 km away from VSC 1. As shown in Fig. 16, the location of DC fault shows minor influence on transients of surge arresters. The peak voltage on sheath (armor) of cable at VSC 2 decreases as fault location approaches to VSC 1.

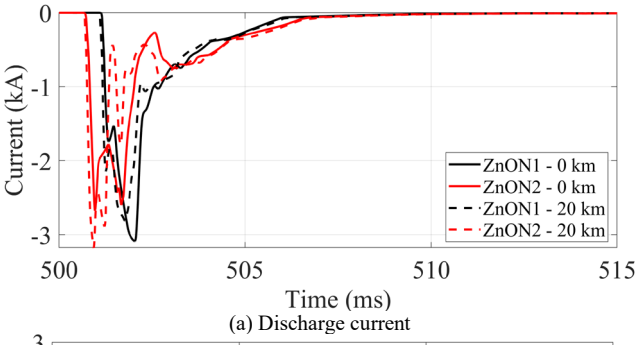

(a) Discharge current

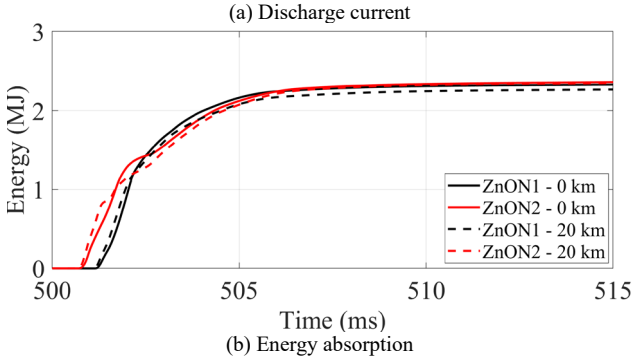

(b) Energy absorption

Fig. 16 Transient characteristics of surge arresters with different DC fault locations.

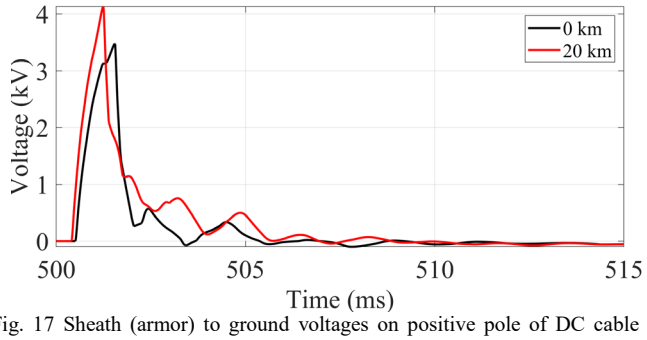

Fig. 17 Sheath (armor) to ground voltages on positive pole of DC cable at VSC 2 with different DC fault locations.

G. Impact of DC cable structure and model

1) Proximity effect due to cable bundle

The DC submarine cable bundle exists strong proximity effect since positive and negative poles are closely touched with each other. As shown in Fig. 18, the proximity effect has no significant impact on energy absorption of two surge arresters. Also, as illustrated in Fig. 2, the main insulation of cable keeps an effective distance between two cores. Thus, the major influence appears on sheath (armor) transient characteristics.

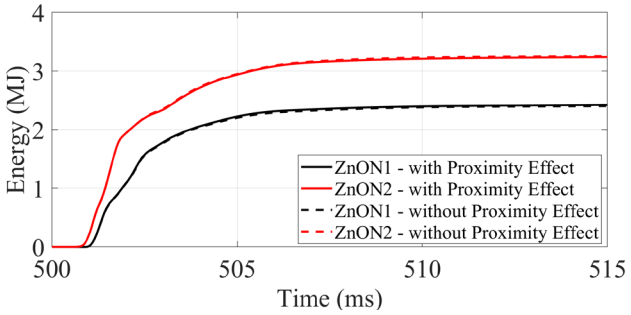

Fig. 18 Energy absorption of surge arresters with impact of proxity effect.

2) Grounding resistance

In this section, the impact of the grounding resistance of sheath (armor) at both ends of DC cable is investigated. The grounding resistance is changed to 0.1 Ω. The transient performance of the surge arrester is illustrated in Fig. 19. In comparison to the results obtained in Fig. 6, no significant influence is observed.

The sheath (armor) transient voltage is shown in Fig. 20. As expected, the voltage decreases as grounding resistance decreases.

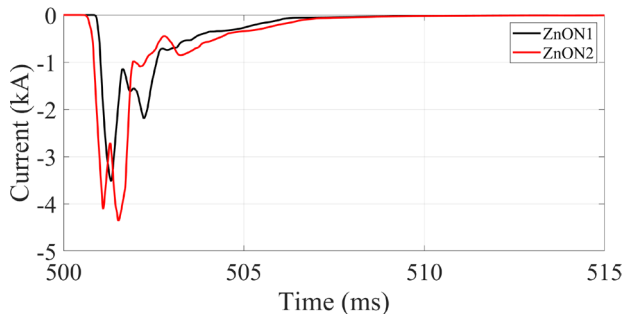

(a) Discharge current

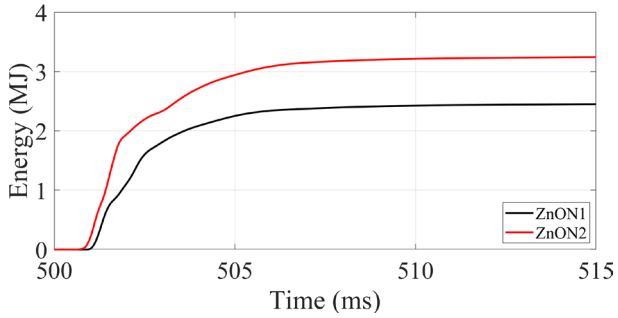

(b) Energy absorption

Fig. 19 Transient characteristics of surge arresters with grounding resistance 0.1 Ω for sheath (armor) of DC cable.

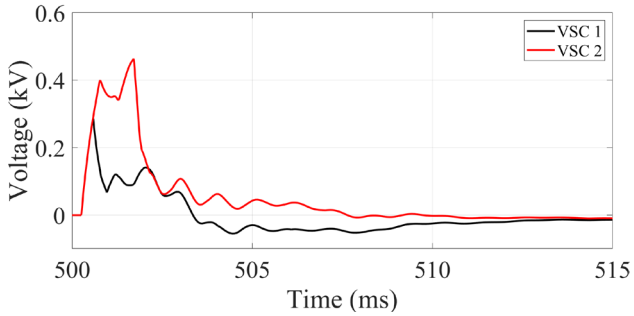

Fig. 20 Sheath (armor) to ground voltages on positive pole of DC cable at VSC 1 and VSC 2 with grounding resistance 0.1 Ω.

3) Model reduction

In the previous sections, each DC cable is modeled using core-sheath-armor structure in detail. In total, it has 6 propagation modes. Next, the Kron reduction is adopted to eliminate the sheath and armor assuming that they are continuously grounded. As a result, only 2 DC pole modes are left. The mode parameters used to build reduced CP cable model [11] is given in TABLE I. The 3 frequencies are used, i.e., 0.1 Hz, 50 Hz and 1 kHz, which approximately match the DC condition, AC steady state and dominant transient frequency component observed in Fig. 4 (b). Thus, the impact of frequency parameters on CP model can be further investigated. The equation (1) defines the current transformation matrix for the two modes propagated in the reduced cable model, i.e., pole-to-pole mode (mode 1) and earth-return mode (mode 2).

$$\mathbf{B} = \begin{bmatrix} 0.71 & 0.71 \\ -0.71 & 0.71 \end{bmatrix} \tag{1}$$

As illustrated in Fig. 21 (a), the DC transient voltages calculated by the reduced WB model agree well with the results produced by the detailed model (see Fig. 4 (b)).

The envelope of DC transient voltages of positive pole generated by the reduced CP model significantly depends on the parameters' frequency. As shown in Fig. 21 (b), the transients cannot be represented by the CP parameters at 0.1 Hz, as expected. As illustrated in Fig. 21 (b), a better performance of transients is achieved if the frequency 1 kHz is adopted. However, a significant deviation in DC steady state is observed, i.e., 341 kV and 319.8 kV at VSC 1 and VSC 2 positive pole, respectively. The reason is from the large deviation in mode resistance calculated at 0.1 Hz and 1 kHz in TABLE I.

As illustrated in Fig. 22, the reduced CP model also shows significant influence on the discharge current and energy of surge arresters. The mismatch of CP model parameters leads to inappropriate transient responses.

TABLE I
MODE PARAMETERS OF CP MODEL (CABLE SEGMENT 5 KM)

Mode	Resistance (Ω)	Surge Impedance (Ω)	Propagation Delay (μs)
f = 0.1 Hz			
1	9.05×10^{-3}	176.29	129.42
2	8.69×10^{-3}	52.79	38.75
f = 50 Hz			
1	7.64×10^{-2}	40.57	29.78
2	3.89×10^{-2}	46.59	34.21
f = 1 kHz			
1	1.44×10^{-1}	36.74	26.97
2	1.41×10^{-1}	36.67	26.92

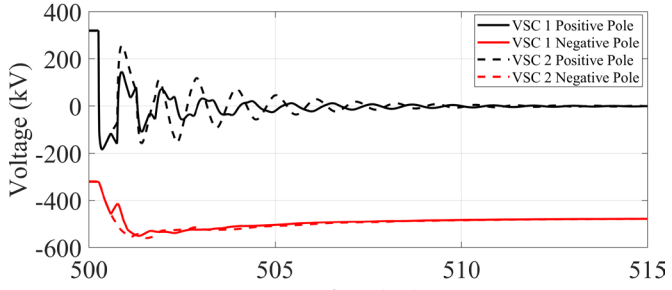

(a) Reduced WB model

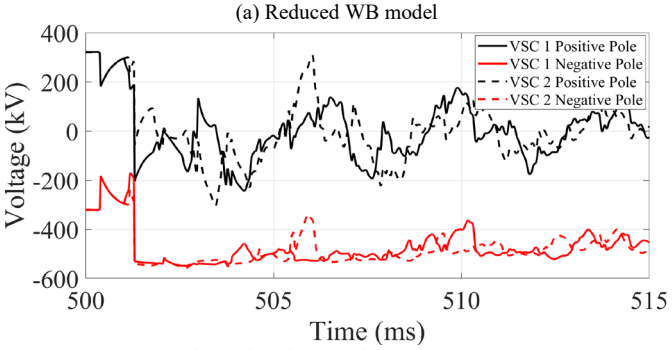

(b) Reduced CP model (f = 0.1 Hz)

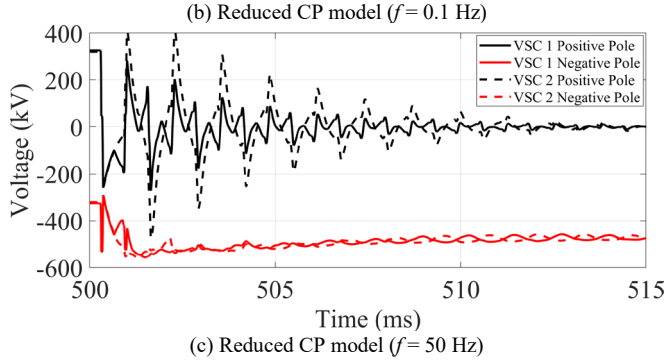

(c) Reduced CP model (f = 50 Hz)

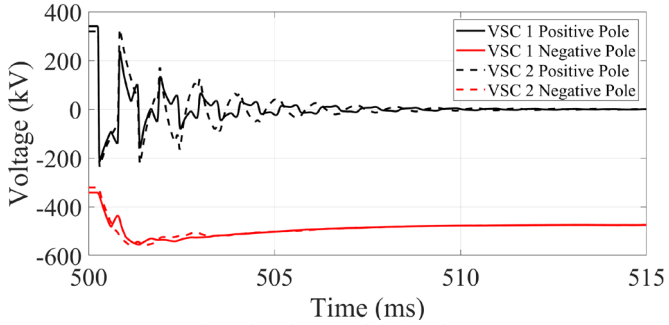

(d) Reduced CP model (f = 1 kHz)

Fig. 21 Pole to ground voltages at VSC 1 and VSC 2.

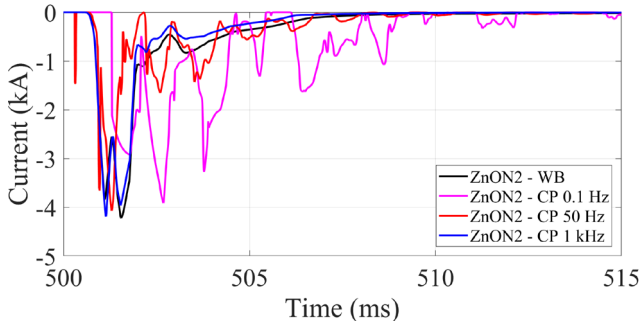

(a) Discharge current

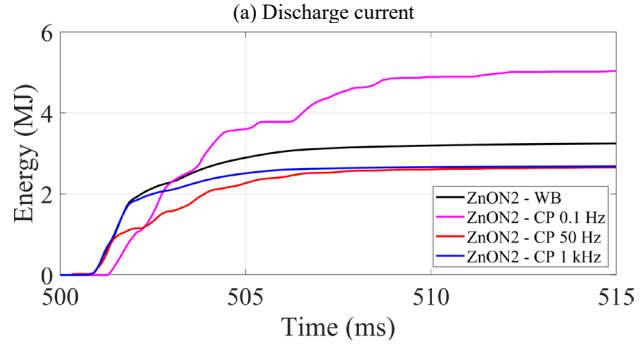

(b) Energy absorption

Fig. 22 Transient characteristics of surge arresters with different cable models.

IV. CONCLUSIONS

This paper has presented investigations on transient characteristics of surge arrester in a typical VSC-HVDC submarine link. The study is based on an EMT-type simulation tool. It has the following brief conclusions.

- Surge arrester can effectively limit the DC overvoltage due to pole to ground fault, i.e., maximum overvoltage -560.1 kV (-1.75 pu). Surge arrester discharge increases overvoltage stress on DC cable sheath (armor).
- Large MMC arm inductance gives more discharges to surge arresters. More critical conditions for energy absorption of surge arrester and sheath (armor) voltage of cable are experienced.
- The reactance of HVDC transformer shows negligible impact on transients of surge arrester.
- The fast blocking time of MMC experiences less discharge current and energy for surge arrester. It has no impact on peak value of DC cable sheath (armor) voltage.
- The discharge energy of surge arrester increases

significantly as transmitted active power increases in the HVDC link. No impact is observed for cable sheath (armor) voltage.

- The DC fault location and proximity effect of cable bundle show minor influence on transients of surge arrester and sheath (armor) voltage.
- The reduced WB and CP models can improve simulation efficiency. However, the results calculated by the reduced CP model are lack of accuracy in comparison to detailed and reduced WB models.
- The results discussed in this paper are based on a specific HVDC system. A comprehensive investigation should be conducted for surge arrester design in different VSC-HVDC submarine links.

V. Appendix

The parameters of HVDC system and DC cable are given in TABLE II and TABLE III.

TABLE II
HVDC Default Data

Rated Power	1000 MVA	AC Frequency	50 Hz
AC Primary Voltage	400 kV	AC Secondary Voltage	340 kV
DC Pole-to-Pole Voltage	640 kV	Transformer Reactance	0.18 pu
Transformer Resistance	0.001 pu	MMC Arm Inductance	0.15 pu
Total Capacitor Energy in Converter	40 kJ/MVA	Number of Submodules/Arm	400
Conduction Losses of Each IGBT/Diode	0.001 Ω	-	

TABLE III
DC Submarine Cable Data

Radius of Core	2.51 cm	Inner Radius of Sheath	6.0 cm
Outer Radius of Sheath	6.2 cm	Inner Radius of Armor	6.51 cm
Outer Radius of Armor	7.06 cm	Outer Radius of Cable	7.56 cm
Resistivity of Core	1.72×10^{-8} Ωm	Resistivity of Sheath	2.74×10^{-7} Ωm
Resistivity of Armor	1.81×10^{-8} Ωm	Relative Permittivity of Insulator	2.3
Resistivity of Seawater	0.2 Ωm	Resistivity of Seawater	10 Ωm

VI. References

[1] CIGRE WG B4-57, *Guide for the Development of Models for HVDC Converters in a HVDC Grid*, Technical Brochure 604, 2014.

[2] K. Sharifabadi, L. Harnefors, H.-P. Nee, S. Norrga and R. Teodorescu, *Design, Control and Application of Modular Multilevel Converters for HVDC Transmission Systems*. Wiley-IEEE Press, 2016.

[3] G. Mazzanti and M. Marzinotto, Extruded Cables For High-Voltage Direct-Current Transmission: Fundamentals of HVDC Cable Transmission. Wiley-IEEE Press, 2013.

[4] J. Peralta, H. Saad, S. Dennetiere, J. Mahseredjian and S. Nguefeu, "Detailed and averaged models for a 401-level MMC–HVDC system," *IEEE Trans. Power Delivery*, vol. 27, no. 3, pp. 1501-1508, 2012.

[5] H. Saad, S. Dennetiere, J. Mahseredjian, P. Delarue, X. Guillaud, J. Peralta and S. Nguefeu, "Modular multilevel converter models for electromagnetic transients," *IEEE Trans. Power Delivery*, vol. 29, no. 3, pp. 1481-1489, 2014.

[6] F. Badrkhani Ajaei and R. Iravani, "Cable surge arrester operation due to transient overvoltages under dc-side faults in the MMC–HVDC link," *IEEE Trans. Power Delivery*, vol. 31, no. 3, pp. 1213-1222, 2016.

[7] H. Wang, J. Cao, Z. He, J. Yang, Z. Han and G. Chen, "Research on overvoltage for XLPE cable in a modular multilevel converter HVDC transmission system," *IEEE Trans. Power Delivery*, vol. 31, no. 2, pp. 683-692, 2016.

[8] M. Goertz, S. Wenig, S. Beckler, C. Hirsching, M. Suriyah and T. Leibfried, "Analysis of cable overvoltages in symmetrical monopolar and rigid bipolar HVDC configuration," *IEEE Trans. Power Delivery*, vol. 35, no. 4, pp. 2097-2107, 2020.

[9] J. Morales, H. Xue, J. Mahseredjian and I. Kocar, "A new tool for calculation of line and cable parameters," *Electric Power Systems Research*, vol. 220, 2023.

[10] H. Xue, J. Mahseredjian, J. Morales, H. Saad, S. Dennetiere and T. Xue, "An investigation of frequency and electromagnetic transient responses on a VSC-HVDC cable network," *IEEE Trans. Power Delivery*, vol. 39, no. 4, pp. 2053-2064, 2024.

[11] A. Ametani, H. Xue, T. Ohno and H. Khalilnezhad, *Electromagnetic Transients in Large HV Cable Networks: Modeling and Calculations*, IET, 2021.

[12] J. Mahseredjian, S. Dennetière, L. Dubé, B. Khodabakhchian and L. Gérin-Lajoie, "On a new approach for the simulation of transients in power systems," *Electric Power Systems Research*, vol. 77, no.11, pp. 1514-1520, 2007.

[13] I. Kocar and J. Mahseredjian, "Accurate frequency dependent cable model for electromagnetic transients," *IEEE Trans. Power Delivery*, vol. 31, pp.1281-1288, 2016.

[14] A. Ramirez, J. Morales, J. Mahseredjian and I. Kocar, "Advanced wideband line / cable modeling for transient studies," *IEEE Trans. Power Delivery*, vol. 39, no. 5, pp. 2956-2964, 2024.

[15] N. Manduley, S. Toure, A, Xemard, B. Raison and S. Poullain, "Effect of the surge arrester configuration in MMC-HVDC systems under DC and converter fault conditions," *International Conference on Power System Transients (IPST)*, Perpignan, 2019.

[16] N. A. M. Rivas, *Contribution to Insulation Coordination Studies for VSC-HVDC Systems*, Ph.D. Thesis, Université Grenoble Alpes, France, 2020.

[17] SIEMENS, *High-Voltage Surge Arresters (Product Guide)*, 2014.

[18] ABB, Exh. TDI-LE-4 (HVDC Cable Design Sheet), http://www.necplink.com/docs/Champlain_VT_electronic/04%20L.%20Eng/Exh.%20TDI-LE-4%20(HVDC%20Cable%20Design%20Sheet%20(ABB)).pdf

[19] R. Shariatinasab, J. Gholinezhad and K. Sheshyekani, "Estimation of energy stress of surge arresters considering the high-frequency behavior of grounding systems," *IEEE Trans. Electromagnetic Compatibility*, vol. 60, no.4, pp.917-925, 2018.

[20] T. C. Bowman, T. Kmieciak and L. B. Biedermann, "Nanosecond transient validation of surge arrester models to predict electromagnetic pulse response," *IEEE Trans. Electromagnetic Compatibility*, DOI:10.1109/TEMC.2024.3486980.

[21] CIGRE JWG B2/B4/C1.17, Impacts of HVDC Lines on the Economics of HVDC Projects, 2009.